Cytometry 11:341–348 (1990)

Intracellular pH, Esterase Activity, and DNA Measurements of Human Lung Carcinomas by Flow Cytometry

F. Liewald, N. Demmel, R. Wirsching, H. Kahle, and G. Valet

Chirurgische Klinik, Klinikum Großhadern der Ludwig-Maximilian-Universität, D-8000 München-Großhadern, Federal Republic of Germany (F.L., N.D., R.W.); Mildred-Scheel-Labor, Max-Planck-Institut für Biochemie D-8033 Martinsried, Federal Republic of Germany (H.K., G.V.)

Received for publication July 21, 1988; accepted July 12, 1989

An important intention of flow cytometric investigations is to obtain biochemical and biophysical information about cells which is suitable for automated tumor diagnosis. In this study, the ploidy status, the intracellular pH value, the intracellular esterase activity, and the cell volume of vital cells and the DNA and cell volume of dead cells were measured in cancerous tissue and normal lung tissue of 30 patients by flow cytometry. The cell samples were simultaneously stained with the pH and esterase indicator dye 1.4-diacetoxy-2,3-dicyanobenzene (ADB) and propidium iodide (PI). The flow cytometric measurements were performed in three-parameter list mode. The data were evaluated on an AT-compatible personal computer with the DIAGNOS1 program system for automated diagnosis of flow cytometric list mode data.

Significant differences were found between normal and malignant tissue in DNA ploidy, in the intracellular esterase activity, in the cell, volume and in the percentage of inflammatory cells and parameters of necrosis. DNA-aneuploidy was observed in 38% of the lung carcinomas. The simultaneous detection of DNA-aneuploidy and tumor-associated properties in a multifactorial analysis led to correct automatic tumor diagnosis in 85% of cases. DNA-aneuploidy was found at a significant higher frequency in advanced tumors. Adenocarcinomas displayed DNA-aneuploidy more often (80%) than squamous cell carcinomas (33%).

Key terms: DNA aneuploidy, automated diagnosis, functional stain

Lung cancers have a poor prognosis (11) because they are difficult to recognize in an early state. X-ray, computer tomography, patient symptoms, and morphological examination of histologic sections are usual diagnostic methods. The development of new procedures for the recognition of abnormal biochemical parameter patterns of lung cells seems of importance to improve early tumor recognition. Flow cytometric measurements detect biochemical abnormalities in individual cells and should be useful in this respect. A flow cytometric parameter which has been frequently measured in lung carcinoma is the cellular DNA. Depending on tumor type and author between 40 and 60% of lung tumors are DNA-aneuploid (2,11). DNA measurements alone, however, are not sufficient for the diagnostic and prognostic evaluation of lung tumors. It was the purpose of this study to measure simultaneously the intracellular pH (14,15), the esterase activity, and the volume of vital cells as well as the DNA and the volume of dead cells by flow cytometry in cells isolated by mechanical dissociation (18) of normal and cancerous tissues of human lung in order to investigate whether determination of cell biochemical parameters of normal and malignant lung cells would increase the diagnostic potential of flow cytometric measurements.

MATERIALS AND METHODS

Patients

Tissue from 8 female and 22 male lung cancer patients with a mean age of 58 years (range 44–72 years) was taken immediately after operation. The tumors were clinically staged according to the criteria of the International Union against Cancer (UICC) and the size of the primary tumor and the degree of lymph node

Table 1
Lung Cancer Classification

	TNM classification					
	T_1	T_2	T_3	N_0	N_1	N_2
Euploid	2	8	1	5	3	3
Aneuploid	1	7	3	3	7	1
	UICC classification					
	I	II	III	IV		
Euploid	5	3	4	—		
Aneuploid	1	2	2	5		

Table 2
Grading and Histology of Lung Cancer

	Grading		
	GI	GII	GIII
Euploid	1	5	5
Aneuploid	1	8	2
	Histology			
	Squamous cell	Adeno	Large cell	Small cell
Euploid	6	2	2	1
Aneuploid	2	8	—	1

infiltration were assessed according to the TNM classification (Table 1). Eight tumors were squamous cell carcinomas, 9 were adeno-, 2 large cell, and 2 small cell lung cancers. The tumor cells were evaluated according to the grading system (Table 2). A pneumonectomy was performed in 8 patients according to the localization and staging of the tumor; 21 patients received a lobectomy and one patient a lower bilobectomy.

Cells

Equal amounts, varying between 0.05 and 0.5g tissue, were removed from the lung cancer tissue and from the normal lung tissue of the same patient. The lung cancer tissue was taken in equal parts from 3 to 5 different locations of non-necrotic tissue. The normal and cancer samples were separately immersed in 0.15 M NaCl solution buffered with 5 mM HEPES to pH 7.35 (HBS-buffer) and cooled to 0–4°C during the following procedures until cell staining or fixation. The tissue samples were minced with a McIlwain electric tissue chopper (The Mickle Comp., Gomshall, England), which was equipped with five parallel razor blades. The chopped tissue was taken up in 5 ml HBS-buffer and sucked 50 times back and forth with a 1 ml Eppendorf plastic tip pipette whose plastic tip was cut at the end to give an opening of 1–1.5 mm diameter. Care was taken to avoid air bubbles. The suspension was filtered through a V2A-steel sieve with 60 μm wire mesh, washed twice by centrifugation in 50 ml HBS at 200*g* for 10 min, and resuspended in 5 ml HBS buffer. The majority of the cells (4.75 ml) were fixed in suspension for later antibody studies by addition of cold methanol to give a final methanol concentration of 70%. Five microliters of a dye cocktail containing 2 mg/ml propidium iodide (PI, Serva, Heidelberg, FRG) and 1 mg/ml 1,4-diacetoxy-2,3-dicyano-benzene (ADB, Paesel, Frankfurt, FRG) were added to the remaining 250 μl of fresh cell sample. PI stains the DNA of dead cells. ADB is cleaved by intracellular esterases by cells with intact membranes into the pH-indicator dye DCH (2,3-dicyano-hydrochinone) and acetate (16). DCH accumulates in cell with intact membranes which are referred to as vital cells. The amount of intracellular DCH fluorescence is a measure of esterase activity and the colour of the emitted fluorescent light indicates the intracellular pH value. The cells were stained for 5 min at room temperature. Monosized, porous, and NH_2-group-bearing particles of 5 μm diameter (Paesel, Frankfurt, FRG) were prestained with 20 μg/ml DCH and added at a final concentration of 2.5×10^5 particles/ml to the cell sample as an internal concentration, fluorescence, and size standard.

Flow Cytometric Measurements

The cell volume and two fluorescences were simultaneously measured with a Fluvo-Metricell flow cytometer (6) (HEKA Elektronik, Lambrecht, FRG). The cell volume was determined from the change of electrical resistance as the cell passed hydrodynamically focused through the center of a cylindrical orifice of 85 μm diameter and 100 μm length, at an electrical current of 0.23 mA. HBS buffer was used as sheath fluid. Fluorescence was excited by an HBO 100 high-pressure mercury arc lamp (Osram, Munich, FRG) between 300 and 400 nm. The emitted cellular fluorescence was collected between 418–440 nm as blue fluorescence of DCH and between 500–750 nm as green fluorescence of DCH and red fluorescence of propidium iodide. The photomultiplier voltage, the amplifier gains, the three-decade logarithmic amplification mode, and the optical filters were kept constant throughout all measurements to maintain constant instrument conditions. The standard position of the monodisperse calibration particles in the histograms was reached by varying the lamp current for the fluorescence measurement and the orifice current for the electric cell volume measurement. All amplifiers were dynamically calibrated over the full range of three logarithmic decades by a series of 7 trapezoid-shaped calibration pulses of 0.1, 0.32, 1.0, 3.2, 10, 32, and 100 mV with a 5 μs rise time, 10 μs length, and a frequency of 1,200 pulses/s. Calibration tables for each logarithmic amplifier were calculated by program CALIB of the DIAGNOS1 program system from list-mode recordings of approximately 21,000 calibration pulses (3,000 pulses/voltage step). The calibration tables were used as look-up tables by the DIAGNOS1 list-mode evaluation program DATLYS.

The maximum amplitudes of the two fluorescence signals and of the volume of each cell were digitized by 128-step analog-digital converters and the digitized values were collected in list mode on a magnetic disc or

on magnetic tape. The data on the tapes were evaluated by the DIAGNOS1 program system (17) (HEKA Elektronik, Lambrecht, FRG) on an AT-compatible personal computer (80286/287 processor, 20 MHz clock speed, 72 Mbyte formatted hard disk, 60 Mbyte casette tape, EGA-graphic card + EGA-color video monitor, MS-DOS 3.30 operating system, standardized GKS-graphics and graphic metafile generating software).

Three-, two-, and one-parameter histograms were calculated from the list-mode data. The three- and two-parameter histograms were displayed as contour graphs. The amplitude scale for the contour lines is logarithmic and covers three decades. The lowest contour line is at the one- or two-cell per channel level in order to display practically all cells of the list-mode measurement. This is important because rare subpopulations of cells might otherwise be lost by inappropriate gating during the quantitative evaluation.

RESULTS

The display of the measured data as a three-dimensional cube gives a quick overview for each cell sample and permits qualitative evaluation of the number of dead and vital cells and the amount of cell debris (Fig. 1A). Morphologically intact cells exhibit both a substantial cell volume signal and either an esterase activity for vital cells or a distinct DNA value and some remainder of esterase activity for dead cells. Bare nuclei show a DNA signal but have only a small volume signal. Enucleated cells appear only with a volume signal in the cell debris. The cube graph also indicates the distribution of the cells into small-volume inflammatory lymphocytes and granulocytes and large-volume epithelial and tumor cells, but the resolution of the various cell clusters is not very good due to the low contour level. A low contour level was chosen in order to prevent inadvertent loss of cell populations with low frequency. Dead cells, debris, and inflammatory cells are more frequent in the cancer cell samples as compared to normal samples.

To obtain better resolution between vital and dead cells, the cube was projected onto its front plane in the blue vs. red fluorescence graph (Fig. 1B). A three-decade logarithmic amplitude scale was used to display all measured cells and particles; i.e., three contour lines outward from the center of a cell cluster corresponds to an amplitude of 10% of the cluster maximum. The diagonal cell cluster (Fig. 1B) contains vital epithelial cells, inflammatory cells, low esterase activity cells, and cell debris. The cluster is reasonably separated from the dead cells which are PI stained and contain variable amounts of the DCH stain. The blue vs. red fluorescence histogram (Fig. 1B) was used for gating the vital cells into the cell volume vs. esterase graph (Fig. 1C) and into the cell volume vs. intracellular pH graph (Fig. 1D). Inflammatory and epithelial cells were distinguishable in the gated histograms by their different cell volume (Fig. 1C,D), esterase activity (Fig. 1C), and intracellular pH (Fig. 1D). The respective mean values in abscissa and ordinate direction for the different cell populations in the various windows of Figure 1B–D were quantitatively determined with the two-parameter evaluation program CALC.

The blue vs. red fluorescence histogram (Fig. 1B) was also used to gate the dead cells into the cell volume vs. DNA histogram (Fig. 2A). The G_0/G_1, S, and G_2/M cell cluster of dead cells in normal and abnormal lung tissue is visible (Fig. 2A). The number and DNA values of the dead cells and of the free nuclei in the G_0/G_1, S, and G_2/M phase of the cell cycle as well as the amount of cells and nuclei with degraded DNA as indicator of necrotic autolysis of Figure 2A were evaluated by program CALC. Program CALC was setting the limits of the evaluation windows individually and automatically according to the following concept: The G_0/G_1 windows of the dead epithelial cells, the inflammatory cells, and the free nuclei were initially set between DNA channel 15 to 45. Program CALC determined the maximum amplitude of the G_0/G_1 peak in each window in a first step. In a second step the window limits were set 2 fluorescence classes above and below the peak amplitude of the G_0/G_1 cell cluster in each window. In a third step the lower limit of the proliferation compartments ($S + G_2/M$ phase cells) and the upper limit of the autolysis compartments were automatically readjusted. The limits of the evaluation windows for cell volume were set for free cell nuclei between channels 5 and 20 (50–260 μm^3), for inflammatory cells between channels 21 and 35 (280–1,430 μm^3), and for epithelial cells between channels 36 and 163 (1,450–45,000 μm^3). By this procedure a fast, reliable, and objective thresholding of the cell volume vs. DNA histograms was achieved without need for human intervention.

Program CALC furthermore determined automatically DNA-aneuploidy. For this purpose the program calculated a projection of the DNA distribution of all cells of the cell volume/DNA histogram (Fig. 2A) or of the epithelial or the inflammatory cells. The resulting DNA distribution was analyzed in the following way: The distribution was scanned to the left and right side of the G_0/G_1 peak and called aneuploid when a discrete DNA peak higher than 25% of the maximum amplitude of the G_0/G_1 phase DNA peak was encountered (Fig. 3A). Shoulders of nearly DNA-euploid cancer cells were not detected by the aneuploidy subroutine of the CALC program. Shoulders in the DNA distributions caused, however, either an abnormally high coefficient of variation (CV) of the G_0/G_1 DNA peak or an abnormally high number of cells in the $S + G_2/M$ proliferation window. Nearly euploid cancer cells in the hypoploid region were only detectable through an increased CV of the G_0/G_1 peak.

A total of 50 parameters were automatically calculated for each measurement from the two parameter histograms of Figure 1B–D and Figure 2A. They were introduced into a database with the procedure DB-PHPI. The database was screened with the procedure LEARN to find the most significant differences be-

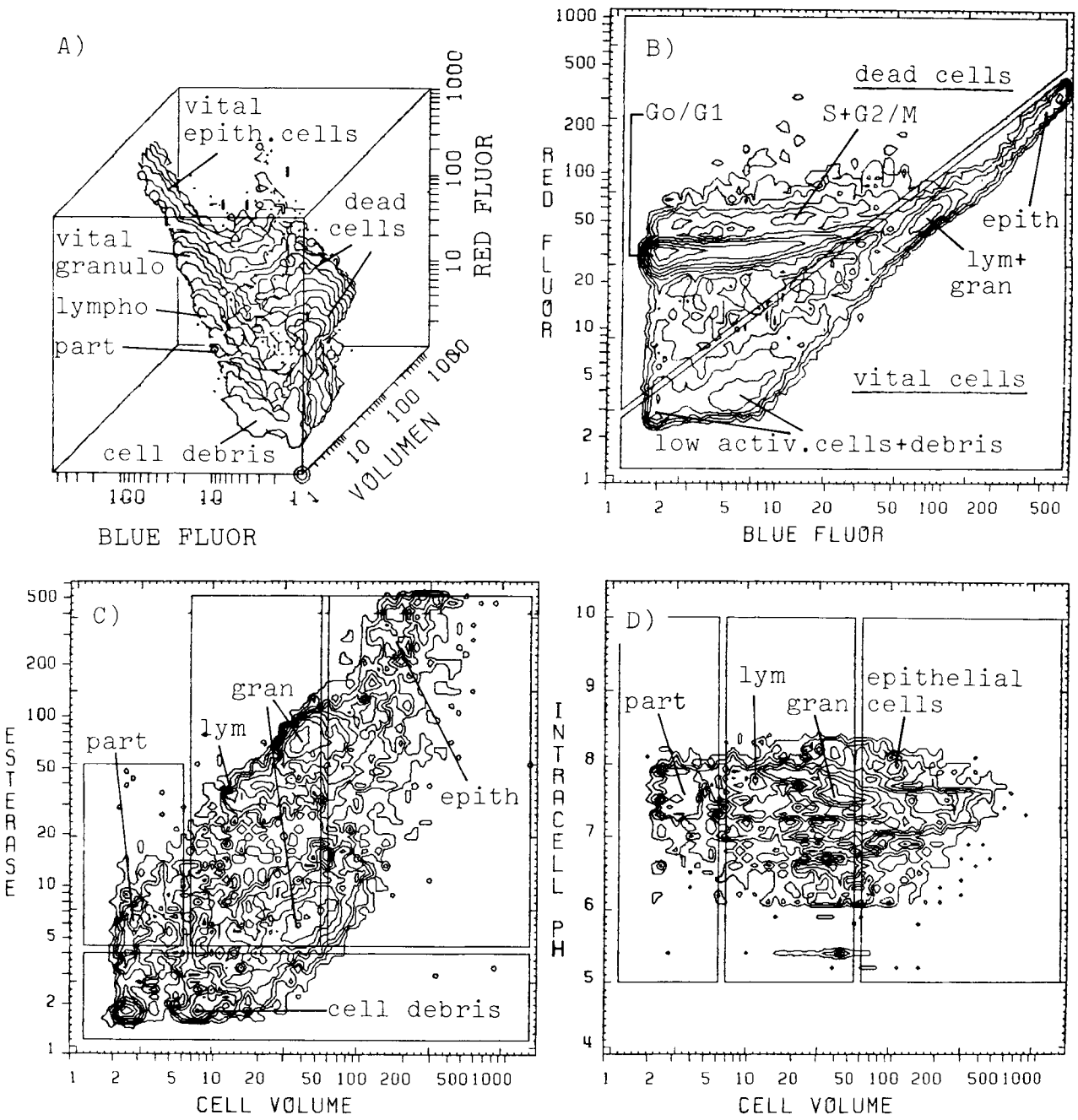

FIG. 1. Cloud display (**A**) of ADB/PI-stained cells of a human lung carcinoma. Vital cells are distinguishable from dead cells and cell debris. The graph is standardized to the maximum logarithmic channel content of the cube (613 cells) and contour lines are plotted at 10% of this level (2 cells/channel). A total of 31,279 cells were measured for this graph. Vital and dead cells were separated for further quantitative evaluation in the blue vs. red fluorescence histogram (**B**) by projection of the cube contents of A onto the front wall of the cube. The graph is standardized to the maximum logarithmic channel content (1,143 cells) and contour lines are plotted from the peak channel downwards in linear steps of 10%. The lowest contour line connects channels with a content of 2 cells; 31,279 cells were collected for the graph. The volume vs. esterase graph (**C**) was obtained by recalculating the list-mode data and gating on the compartment of vital cells. The number of inflammatory cells (lymphocytes and granulocytes), of calibration particles, and of the amount of cell debris was numerically evaluated. Very different and heterogeneous cellular esterase activities were observed for lymphocytes and granulocytes. The graph contains 7,637 cells with 58 cells in the maximum channel. One logarithmic volume class corresponds to a volume of 26 μm^3. The volume vs. intracellular pH graph (**D**) was obtained by gating on the compartment of vital cells of B. The pH value was calculated from the blue vs. red fluorescence ratio of each cell by using a calibration curve in the computer program DATLYS as look-up table. The wide range of intracellular pH values of inflammatory and epithelial cells is noticeable. The graph contains 6,262 cells with a maximum channel content of 97 cells.

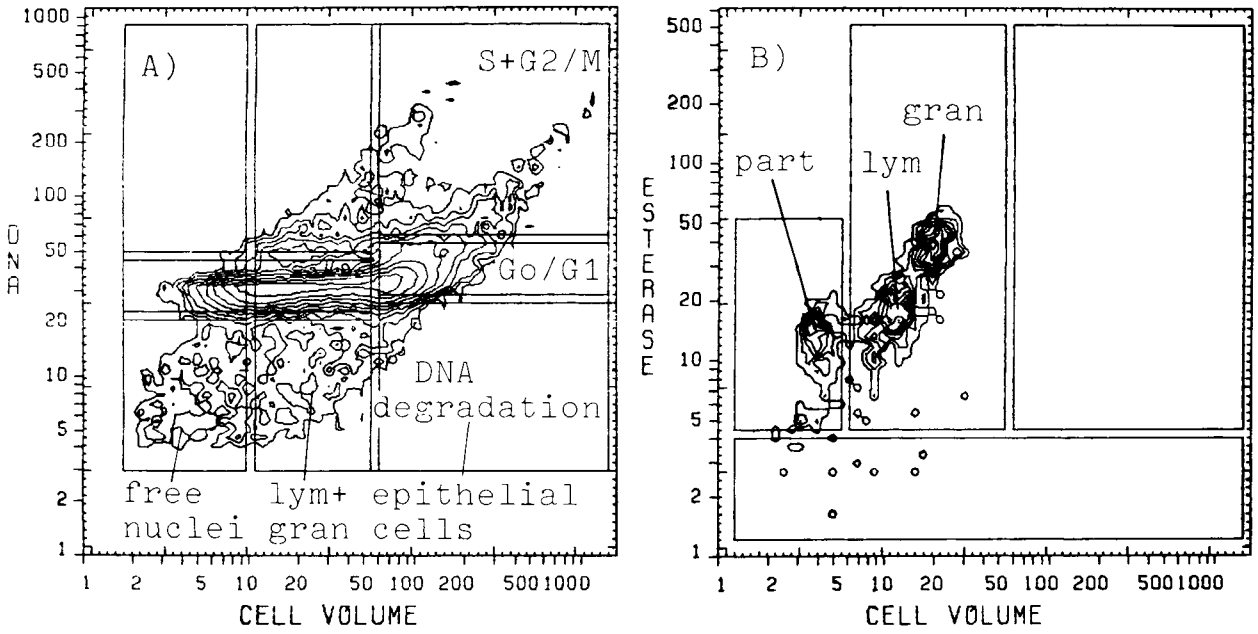

FIG. 2. The cell volume vs. DNA graph of dead cells **(A)** was obtained by gating on the dead cells compartment of Figure 1B. The DNA distribution of the epithelial cells, of the inflammatory cells, and of the free nuclei was evaluated for the G_0/G_1 phase and for the $S+G_2/M$ proliferation compartments. DNA degradation as an indicator of tumor cell necrosis and autolysis was estimated from the areas below the G_0/G_1 phases. The cell volume vs. esterase activity of lymphocytes and granulocytes from fresh cubital vein blood (5 U/ml heparin) **(B)** were stained with the ADB/PI dye cocktail for comparison with the inflammatory cell compartment of the lung cell suspensions. Cell clusters are observed in the peripheral blood similar to those in the lung cell suspension (Fig. 1C). The lymphocytes and granulocytes in the peripheral blood are smaller than in the lung tissue. The lymphocytes and granulocytes in the lung (Fig. 1C) contain either higher or significantly lower esterase activities than the peripheral blood cells, which may indicate different functional states. The cellular fluorescences are directly comparable, although the calibration particles show a lower modal fluorescence in Figure 1C (fluorescence class 18) as compared to B (class 28). The differences of the position of the calibration particles in the histograms are due to fluorescence differences between different batches of calibration particles. The graphs (A,B) contain 23,307 and 616 cells and particles with maximum channel contents of 439 and 28 cells.

tween samples from lung cancer and normal lung tissue.

The procedure LEARN of the DIAGNOS1 program system calculated the mean of each of the 50 database columns for all cell samples from normal and cancerous lung tissue (Table 1). The five data columns with the most significantly different mean values were introduced into a second database, standardized to the mean of the normals as 100%, and subjected to a multifactorial analysis. The multifactorial analysis generated an additional 26 data columns which were stored in the second database. The total of 31 data columns in the second database were screened like the original database by the same procedure, LEARN, for the most significantly different data columns. Aneuploidy and the three data columns of the multifactorial database with the greatest differences between normal and abnormal samples were automatically chosen by procedure LEARN as diagnostic indicators. A sample was classified abnormal when one of the four diagnostic indicators was outside the normal range at a specificity level of 90%. A total of 22 of the 26 samples were classified as abnormal, which corresponds to a sensitivity level of 85% for the automated classification. Four samples of the 30 samples were rejected because they contained less than 200 epithelial cells. Computing time for list-mode analysis and diagnosis was approximately 2 min/patient sample.

Tumor samples contained fewer vital cells but more vital epithelial cells than normal lung tissue (Table 3). The cell volume, esterase activity, and esterase activity concentration of tumor cells were lower than in normal tissue. The intracellular pH was slightly elevated in malignant cells. The cell volume, esterase activity, esterase activity concentration, and intracellular pH were elevated in inflammatory cells. Eleven of the 26 malignant cell samples (42.3%) contained DNA-aneuploid cells (Table 3). Mainly advanced tumors in T_2, T_3, or stage III and IV or tumors with a histologic grading of G II were aneuploid. Aneuploidy was frequently associated with lung adenocarcinomas (Table 2).

DISCUSSION

The evaluation of the flow cytometric list mode data in this study was made automatically by the DIAGNOS1 program system. The evaluation included automated thresholding for cell volume/DNA histograms (Fig. 2A) and automated aneuploidy detection. Due to the complex cell composition of normal and cancerous lung tissue some overlap between inflammatory

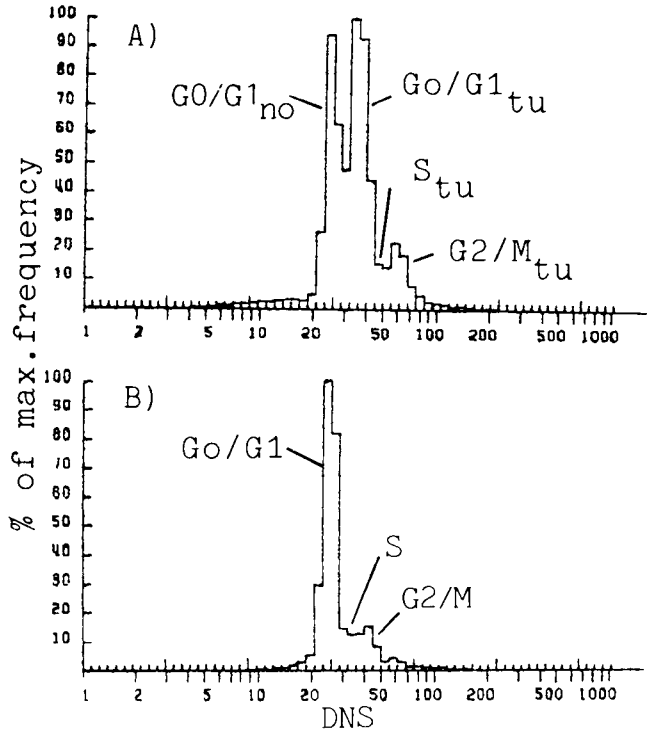

FIG. 3. DNA distribution of cells of a human lung carcinoma (**A**) and of the normal lung tissue (**B**) of the same patient. The separate peak of the DNA-aneuploid cells in the tumor sample (A) is visible. The DNA index of the aneuploid cells is 1.42. A total of 32,371 (A) and 15,330 (B) cells were measured with maximum channel contents of 5,497 and 4,994 cells.

and epithelial cells exists in various two-parameter histograms (Figs. 1B–D, 2A). The overlaps seem more important than they are in reality. They are overemphasized by the three-decade logarithmic amplitude scale of the graphs, which was chosen to display all cells and particles of each measurement. Three adjacent contour lines correspond to one amplitude decade; i.e., histogram channels at the fourth contour line from a cell cluster maximum are below 10% of the maximum amplitude value.

The existing overlap does not substantially influence the results, because the conditions for measurement and evaluation were well standardized from day to day and equal for all samples. The differentiation between cells with intact membranes and dead cells (Fig. 1B) was possible because dead cells contained sufficient PI red fluorescence besides residual DCH blue fluorescence to separate them from cells with intact membranes. The cells containing DCH but no PI are considered as vital cells. The position of the lymphocyte-granulocyte clusters and of calibration particles in the two-parameter histograms (Fig. 1B,C) is known from previous experiments with cells from human colorectal cancers (15,19) and from cytostatic drug testing on patient tumor cells (15). Furthermore the positions of particles and inflammatory cells were identified by measurements on peripheral blood cells (Fig. 2B) (10).

DNA-aneuploidy is considered as a certain indicator for malignant transformation in a tumor. Frankfurt et al. (3) observed 66% aneuploid cases in 430 solid human tumors with 61% DNA-aneuploidy among primary tumors and 71% among metastatic tumors. Small-cell lung carcinomas were found to be aneuploid in about 69% (18). Only 38% of the lung cancers in our study provided evidence for DNA-ploidy aberrations.

The discussion about the correlation between aneuploidy and the clinical staging and grading of a tumor is controversial. Teodori et al. (11) examined 150 tumor specimens from 49 patients with non-small-cell lung carcinomas. In their study the ploidy level could not be correlated with clinical parameters such as tumor stage. Other authors described, however, a linkage between depth of invasion, node status, and DNA ploidy in colon and breast cancer (1,8,12). In our study five of six lung tumors at stage I showed a diploid DNA level. All lung tumors at stage IV were aneuploid (Table 1). One reason for the discrepancy may be organ-specific differences of tumors. In cancer of the bladder and prostate (5,13,14) a relationship between aneuploidy and tumor stage was demonstrated. Such a correlation has also been shown in colorectal cancer by some authors (19), but not by others (9).

The grade of tissue differentiation in the present study was not correlated with the level of ploidy (Table 2). This gives the possibility for clinical and prognostic applications of these data. According to Frankfurt (3–5) poorly differentiated tumors may be subclassified into diploid and aneuploid groups and clinical behaviour of these two groups may be compared.

Four different histological types are most often diagnosed in lung cancer: small-cell carcinoma, large-cell carcinoma, squamous cell carcinoma, and adenocarcinoma. In our study a relationship between the aneuploidy and the histological type was evaluated by applying the chi-square test. Six of 8 squamous cell carcinomas were DNA diploid ($P < 0.01$); 7 of 9 adenocarcinomas were DNA aneuploid. This indicates a preference of DNA-aneuploidy in lung adenocarcinomas. Since aneuploidy is not present in all tumors, additional cell parameters are necessary to increase tumor cell recognition by flow cytometric procedures. One objective of this study was to improve the automated recognition of tumor samples by flow cytometry. Following the simultaneous measurements of intracellular pH, esterase activities, cell volume, and DNA of epithelial and inflammatory cells, a multiparameter calculation of the measured data was performed. In the present study 84% of the tumors were correctly diagnosed at a specificity level of 90% by fully automated operation. This is substantially more than by DNA-aneuploidy alone (39%). The practical question remains whether flow cytometry with automated evaluation can be developed for routine clinical and research application. The false-negative results of 16% show that a single flow cytometric measurement cannot replace histopathological examination.

Table 3
Mean Values and Standard Error of Cell Biochemical Parameters in Normal Lung Tissue and Lung Cancer

	Tumor n = 26	Normal n = 13	$P<$*
Vital cells			
% of all cells	31.0 ± 2.7	47.0 ± 3.7	0.01
% vital inflam. cells	80.4 ± 2.8	86.2 ± 2.1	0.1
% vital epith. cells	19.6 ± 2.8	13.8 ± 2.1	0.1
Dead cells			
% dead of all inflam. cells	67.4 ± 3.1	52.6 ± 4.1	0.05
% dead of all epith. cells	70.7 ± 3.8	56.1 ± 3.9	0.05
Epithelial cells			
Cell volume	3.01 ± 0.16	3.49 ± 0.18	0.1
Esterase activity	0.71 ± 0.09	1.13 ± 0.19	0.05
Esterase concentration	0.24 ± 0.03	0.31 ± 0.05	0.1
pH	7.48 ± 0.04	7.43 ± 0.04	0.5
% S + G_2/M	26.5 ± 2.8	31.9 ± 3.8	0.1
% debris	17.6 ± 3.2	16.8 ± 5.5	1.0
Inflammatory cells			
Cell volume	0.58 ± 0.02	0.47 ± 0.03	0.05
Esterase activity	0.23 ± 0.03	0.20 ± 0.02	0.5
Esterase concentration	0.51 ± 0.11	0.52 ± 0.06	1.0
pH	7.42 ± 0.05	7.34 ± 0.04	0.1
% S + G_2/M	23.2 ± 3.2	26.2 ± 2.8	0.1
% debris	10.9 ± 2.2	8.2 ± 2.8	0.1
Free nuclei			
% of all DNA contain. part.	32.9 ± 3.8	48.3 ± 3.4	0.05

*P, Student's t-test.

To improve the present sensitivity it is possible to stain several aliquots of cell suspension with different biochemical stains, including fluorescent antibodies. The most different data columns of each database can then be jointly evaluated in a new database. Such a database with the multifunctional parameter pattern of normal and lung cancer cells should increase both specificity and sensitivity levels for the identification of cancer cells.

Flow cytometry and multiparameter evaluation make it possible to perform fast and quantitative biochemical analyses in single cells and to detect alterations in cell metabolism in tumorous transformation. Significant differences between normal lung tissue and lung cancer were observed in this study. The esterase activity was lower ($P < 0.05$) in the cancerous cells than in normal lung epithelial cells. In the areas of cancerous lesion the frequency of inflammatory cells and also the cell volume of the inflammatory cells were significantly increased. The greater cell volume may represent a higher biologic activity in the course of the digestion of necrotic material. Samples from cancerous areas also contain a higher degree of dead cells and cell debris (Table 3).

The results show that significant biochemical differences exist between normal and cancerous lung tissue. These differences are useful for diagnosis because more samples are recognized as abnormal than by DNA measurements alone. It is also possible that the biochemical parameter pattern may carry prognostic information with regard to speed of tumor growth or likelihood of metastases. It is, therefore, of interest to extend the knowledge of functional biochemical abnormalities in human tumors.

LITERATURE CITED

1. Banner BF, Tomas de la Vega JE, Roseman DL, Coon JS: Should flow cytometric DNA analysis precede definitive surgery for colon carcinoma? Ann Surg 202(6):740–744, 1985.
2. Bunn PA, Carney DN, Gazdar AF, Whang-Peng J, Matthews MJ: Diagnostic and biological implications of flow cytometric DNA content analysis in lung cancer. Cancer Res 43:5026–5032, 1983.
3. Frankfurt OS, Slocum HK, Rustum YM, et al.: Flow cytometric analysis of DNA aneuploidy in primary and metastatic human solid tumors. Cytometry 5:71–80, 1984.
4. Frankfurt OS: Assessment of cell viability by flow cytometric analysis using DNase exclusion. Exp Cell Res 144:478–482, 1983.
5. Frankfurt OS, Huben RP: Clinical applications of DNA flow cytometry for bladder tumors. Urology 23(Suppl 3):29–34, 1984.
6. Kachel V, Glossner E, Kordwig E, Ruhenstroth-Bauer G: Fluvo-Metricell, a combined cell volume and cell fluorescence analyzer. J Histochem Cytochem 25:804–812, 1977.
7. Kachel V, Schneider H: On line-three parameter data uptake, analysis and display device for flow cytometry and other applications. Cytometry 7:25–40, 1986.
8. Rognum TO, Thorud E, Brandtzaeg P: Preservation of cytometric DNA distribution and epithelial marker expression after tumor progression of human large bowel carcinomas. Cancer 56:1658–1666, 1985.
9. Rognum TO, Thorud E, Elgjo K, Brandtzaeg P, Orjasaeter H, Nygaard K: Large bowel carcinomas with different ploidy, related to secretory component, IgA and CEA in epithelium and plasma. Br J Cancer 45:921–934, 1982.
10. Rothe G, Valet G: Phagocytosis, intracellular pH and cell volume in the multifunctional analysis of granulocytes by flow cytometry. Cytometry 9:316–324, 1988.

11. Teodori L, Tirindelli-Danesi D, Mauro F, et al.: Non small cell lung carcinoma: Tumor characterization on the basis of flow cytometrically determined cellular heterogeneity. Cytometry 4: 174–183, 1983.
12. Thorud E, Fossa SD, Vaage S, Kaalhus O, Knudsen OS, Bormer O, Shoaib MC: Primary breast cancer: Flow cytometric DNA pattern in relation to clinical and histopathologic characteristics. Cancer 57:808–811, 1986.
13. Tribukait B, Gustafson H: Impulscytometrische DNS-Untersuchungen bei Blasenkarzinomen. Onkologie 6:278–288, 1980.
14. Tribukait B, Hammarberg C, Rubio C: Ploidy and proliferation patterns in colorectal adenocarcinomas related to Dukes classification and to histopathological differentiation. Acta Pathol Microbiol Immunol Scand [A] 91:89–95, 1983.
15. Valet G, Raffael A: Determination of intracellular pH and esterase activity in vital cells by flow cytometry. In: Cytostatic Drug Testing on Patient Tumor Cells, Valet G (ed). Paesel, Frankfurt, 1984, pp 3–21.
16. Valet G, Raffael A, Moroder L, Wünsch E, Ruhenstroth-Bauer G: Fast intracellular pH determination in single cells by flow cytometry. Naturwissenschaften 68:265–266, 1981.
17. Valet G: Automated diagnosis of malignant and other abnormal cells by flow cytometry using newly developed DIAGNOS1 program system. In: Proc. Int. Symp. Clin. Cytometry and Histometry, Burger G, Ploem B, Goerttler K (eds). Academic Press, London, 1987, pp 58–65.
18. Vindelov LL: Flow microfluorometric analysis of nuclear DNA in cells from solid tumors and cell suspensions. Virchows Arch [B] 24:227–242, 1977.
19. Wirsching R, Lamerz R, Wiebecke B, Liewald F: Flow cytometric evaluation of colorectal carcinoma as completion of conventional tumor examination. J Exp Clin Cancer Res 6(2):117–125, 1987.